⌘ *Author's Choice*

THE JOURNAL OF BIOLOGICAL CHEMISTRY VOL. 286, NO. 49, pp. 42736–42748, December 9, 2011

Functional Properties of a Newly Identified C-terminal Splice Variant of $Ca_v1.3$ L-type Ca^{2+} Channels*[S]

Received for publication, June 9, 2011, and in revised form, July 21, 1011 Published, JBC Papers in Press, October 13, 2011, DOI 10.1074/jbc.M111.269951

Gabriella Bock[‡1], Mathias Gebhart[‡1], Anja Scharinger[‡], Wanchana Jangsangthong[§], Perrine Busquet[‡], Chiara Poggiani[‡], Simone Sartori[‡], Matteo E. Mangoni[¶‖‡‡], Martina J. Sinnegger-Brauns[‡], Stefan Herzig[§], Jörg Striessnig[‡2], and Alexandra Koschak[‡3]**

From the [‡]Institute of Pharmacy, Pharmacology and Toxicology and Center of Molecular Biosciences Innsbruck, Peter-Mayr-Strasse 1/I, A-6020 Innsbruck, Austria, the [§]Department of Pharmacology and Center for Molecular Medicine, University of Cologne, Gleueler Strasse 24 and Robert-Koch-Strasse 21, D-50931 Cologne, Germany, the [¶]Département de Physiologie, CNRS, UMR-5203, Institut de Génomique Fonctionnelle, F-34000 Montpellier, France, [‖]INSERM, U661, F-34000 Montpellier, France, the [**]Universités de Montpellier 1 & 2, UMR-5203, F-34000 Montpellier, France, and [‡‡]INSERM, U637, Montpellier, France

An intramolecular interaction between a distal (DCRD) and a proximal regulatory domain (PCRD) within the C terminus of long $Ca_v1.3$ L-type Ca^{2+} channels ($Ca_v1.3_L$) is a major determinant of their voltage- and Ca^{2+}-dependent gating kinetics. Removal of these regulatory domains by alternative splicing generates $Ca_v1.3_{42A}$ channels that activate at a more negative voltage range and exhibit more pronounced Ca^{2+}-dependent inactivation. Here we describe the discovery of a novel short splice variant ($Ca_v1.3_{43S}$) that is expressed at high levels in the brain but not in the heart. It lacks the DCRD but, in contrast to $Ca_v1.3_{42A}$, still contains PCRD. When expressed together with $\alpha2\delta1$ and $\beta3$ subunits in tsA-201 cells, $Ca_v1.3_{43S}$ also activated at more negative voltages like $Ca_v1.3_{42A}$ but Ca^{2+}-dependent inactivation was less pronounced. Single channel recordings revealed much higher channel open probabilities for both short splice variants as compared with $Ca_v1.3_L$. The presence of the proximal C terminus in $Ca_v1.3_{43S}$ channels preserved their modulation by distal C terminus-containing $Ca_v1.3$- and $Ca_v1.2$-derived C-terminal peptides. Removal of the C-terminal modulation by alternative splicing also induced a faster decay of Ca^{2+} influx during electrical activities mimicking trains of neuronal action potentials. Our findings extend the spectrum of functionally diverse $Ca_v1.3$ L-type channels produced by tissue-specific alternative splicing. This diversity may help to fine tune Ca^{2+} channel signaling and, in the case of short variants lacking a functional C-terminal modulation, prevent excessive Ca^{2+} accumulation during burst firing in neurons. This may be especially important in neurons that are affected by Ca^{2+}-induced neurodegenerative processes.

In electrically excitable cells different types of voltage-gated Ca^{2+} channels convey activity-dependent intracellular Ca^{2+} signals with high spatial and temporal control. Such Ca^{2+} signals are adjusted to specific cellular needs through many different mechanisms. At least 10 $\alpha1$ subunit isoforms form the Ca^{2+}-selective pore of voltage-gated Ca^{2+} channels providing diversity through differences in their biophysical properties, the distribution within specialized plasmalemmal compartments, protein interaction partners, and regulation by second messenger pathways (1). Thereby voltage-gated Ca^{2+} channels divert Ca^{2+} signals to different cellular processes within the same cell. For instance, presynaptic $Ca_v2.1$, $Ca_v2.2$, and $Ca_v2.3$ trigger fast neurotransmitter release in neurons, whereas somatodendritic L-type Ca^{2+} channels (LTCCs)[4] ($Ca_v1.2$, $Ca_v1.3$) can signal to transcriptional events and induce long lasting alterations of neuronal responsiveness (2, 3). Likewise, in mouse pancreatic β-cells the fast phase insulin release is under the control of $Ca_v1.2$ channels, whereas the slow phase requires Ca^{2+} influx through $Ca_v2.3$ channels (1, 4).

More recently, alternative splicing has been identified as another important regulator of voltage-gated Ca^{2+} channel-mediated signaling. Alternative splicing in the proximal C terminus of the $Ca_v2.2$ $\alpha1$ subunit of N-type channels changes the dynamics of $G_{i/o}$ protein-dependent inhibition resulting in an altered analgetic response to spinal morphine (5). Alternative splicing of $Ca_v1.2$ $\alpha1$ subunits can generate variants with more hyperpolarized window currents likely to support basal myogenic tone in arterial vascular smooth muscle (6).

We have recently discovered an automodulatory domain within the C terminus of $Ca_v1.4$ and $Ca_v1.3$ L-type Ca^{2+} channels (7–9), which tightly controls the gating behavior of these channels. This C-terminal modulator (CTM) consists of two putative α-helices (8) in the proximal (PCRD) and distal (DCRD) C terminus and interaction between the DCRD and the PCRD is required for CTM function. The CTM strongly reduces calmodulin (CaM)-dependent Ca^{2+}-dependent inactivation (CDI) of $Ca_v1.3$ channels and promotes their activation

* This work was supported, in whole or in part, by National Institutes of Health Grant R01HL087120-A2, Austrian Science Fund (FWF) Grants P-22528 (to A. K.) and P-20670 and F4402 (to J. S.), The European Community Research Training Network Cavnet Grant MRTN-CT-2006-35367), Center for Molecular Medicine Cologne Grant CMMC A5 (to S. H.), and the University of Innsbruck.

[S] The on-line version of this article (available at http://www.jbc.org) contains supplemental Figs. S1 and S2 and Table S1.

⌘ *Author's Choice*—Final version full access.

[1] Both authors contributed equally to this work.

[2] To whom correspondence may be addressed. Tel.: 43-512-507-5600; Fax: 43-512-507-2931; E-mail: joerg.striessnig@uibk.ac.at.

[3] To whom correspondence may be addressed: Center for Physiology and Pharmacology, Dept. of Neurophysiology and -pharmacology, Währinger-strasse 13A, A-1090-Wien, Austria. Tel.: 43-1-4277-64150; Fax: 43-01-4277-9641; E-mail: alexandra.koschak@meduniwien.ac.at.

[4] The abbreviations used are: LTCC, L-type Ca^{2+} channel; CDI, calcium-dependent inactivation; CaM, calmodulin; CTM, C-terminal modulator; PCRD, proximal C-terminal regulatory domain; DCRD, distal C-terminal regulatory domain; HP, holding potential; APW, action potential waveform; ANOVA, one-way analysis of variance; SAN, sinoatrial node; SN, substantia nigra.

at more negative voltages (8). Because this negative activation range of $Ca_v1.3$ channels is a prerequisite for their dominant role in sinoatrial node pacemaking, hearing, and for shaping neuronal excitability (1, 10, 11) the CTM appears to have a special role in adjusting $Ca_v1.3$-mediated Ca^{2+} entry. This suggestion is further supported by the fact that alternative splicing of exon 42 can give rise to a $Ca_v1.3$ $\alpha1$ subunit with a long ($Ca_v1.3_L$, previously (see Ref. 8) referred to as $Ca_v1.3_{42}$) and a short C terminus ($Ca_v1.3_{42A}$). The latter retains the interaction motifs for CaM but lacks the PCRD and DCRD (8). Using a quantitative PCR approach we demonstrated that $Ca_v1.3_{42A}$ mRNA is expressed at lower levels than $Ca_v1.3_L$ in whole brain, individual brain regions, and in the heart. $Ca_v1.3_{42A}$ channels expressed in tsA-201 cells almost completely lack capacitative ON gating currents (Q_{ON}) despite robust Ca^{2+} inward current (I_{Ca}) (8). Although not yet substantiated by single channel recordings, this suggests a higher channel open probability (P_{open}) or single channel conductance. Thus more pronounced activity may allow this short variant to contribute substantial I_{Ca} despite its expected lower expression level.

Here we addressed several important questions regarding the potential physiological significance of alternative splicing within the CTM for $Ca_v1.3$ function. We describe a novel splice variant ($Ca_v1.3_{43S}$) abundantly expressed in the brain but not in heart tissue. This short splice variant lacks the DCRD and therefore a functional CTM. The gating properties of $Ca_v1.3_{43S}$ differ slightly from $Ca_v1.3_{42A}$ due to the presence of the PCRD, which permits modulation by C-terminal fragments derived from $Ca_v1.2$ channels. Single channel analysis revealed that P_{open} strongly increases in the absence of a functional CTM but with no change of the single channel conductance. We further demonstrate that C-terminal splicing changes I_{Ca} during stimuli simulating short bursts of action potentials. Taken together our data reveal functional differences between all alternatively spliced $Ca_v1.3$ channel variants investigated in this study that are important for the understanding of their differential function in physiological and probably also in disease states.

EXPERIMENTAL PROCEDURES

RNA Preparation, Reverse Transcription, and PCR

Human brain total RNA was purchased from Clontech (Saint-Germain-en-Laye, France). tsA-201 cells were trypsinized on the third day after transfection, washed two times in PBS, and then processed immediately. Mouse tissue was dissected from adult (6–12 months) male C57B/6N animals as published (12, 13), shock frozen in liquid nitrogen, and stored at −80 °C. Total RNA was purified from tissue pools (heart and brain regions) or individual samples using the RNAqueus®-4PCR Kit and DNase I (brain regions and tsA-201 cells; Ambion, Foster City, CA), the Qiagen RNeasy Lipid Tissue Kit (whole brain and brain regions; Qiagen), and the Qiagen RNeasy Fibrous Tissue Kit (whole heart and heart regions) according to the manufacturer's protocols. The RNA concentration was measured using Nanodrop, and RNA quality was evaluated via separation of 28 S and 18 S rRNA bands on a denaturing agarose gel. One μg of total RNA was reverse transcribed at 42 °C (RevertAid™ H Minus First Strand cDNA Synthesis Kit, Fermentas, St. Leon-Roth, Germany) or 55 °C (RevertAid™ Premium First Strand cDNA Synthesis Kit, Fermentas) with random hexamer or oligo(dT) primers in a reaction volume of 20 μl. The concentration of the cDNA was referred to in RNA equivalents, *i.e.* 1 μl of reverse transcription reaction (cDNA) was equal to 50 ng of RNA. To amplify fragments containing exon 43, 20–100 ng of RNA equivalent was used in qualitative splice variant analysis with PCR, with primers specific for human (GenBank™ accession number EU363339; forward, 5′-AACCCTGTTTGCTTTGGTTC-3′; reverse, 5′-GCAGCTTTGGACATATTGGC-3′) and mouse $Ca_v1.3$ $\alpha1$ subunit (NM_001083616.1; forward, 5′-CGAGCCAGAAGACTCCAAA-3′; reverse, 5′-CACAGCACTCCTCGCTACTG-3′). Alternative splicing of exon 41 was detected using reverse primers specific for exon 42 (5′-TATAGCACGCCGGATTTCTG-3′) or exon 42A (5′-CCACCTTCCGGAGGAGTG-3′). PCRs were performed using PCR Master Mix (2 times) (Fermentas) in the presence of 5% (v/v) dimethyl sulfoxide (for fragments containing exon 43; 95 °C for 5 min, 35 cycles of 92 °C for 30 s, 58 °C for 30 s, 72 °C for 1 min) or with BioTherm™ *Taq* DNA Polymerase (GeneCraft, Lüdinghausen, Germany) in the presence of 1.5 mM $MgCl_2$ (for fragments containing exon 41; 94 °C for 3 min, 40 cycles of 94 °C for 45 s, 55 °C for 45 s, and 68 °C for 1 min, followed by an elongation step of 68 °C for 10 min). Primers detecting GAPDH were used for positive control: mouse, GenBank accession number NM_008084, forward primer, 5′-ACTCCACTCACGGCAAATTC-3′, reverse primer, 5′-CACATTGGGGGTAGGAACAC-3′; human, GenBank accession number NM_002046, forward primer, 5′-CAATGACCCCTTCATTGACC-3′, reverse primer, 5′-GAGGCAGGGATGATGTTCTG-3′. Samples without template were used as negative control. PCR products containing exons 43S or 43L were ligated into pGEM-T Easy vector (Promega, Mannheim, Germany), verified by sequencing (MWG Biotech), and subsequently also employed as positive and negative control templates in PCR. Theoretically, 43S PCR fragments could have been derived from cDNA that reflects unresolved secondary structures in the RNA region coding exon 43. Therefore, conditions that would relax the secondary structure (reverse transcription at 55 °C, PCR in the presence of 5% (v/v) dimethyl sulfoxide) should prevent amplification of 43S if it arose merely as a structural artifact. We could, however, detect 43S under these conditions (Fig. 1*b*). As a further control we also harvested RNA from tsA-201 cells that transiently expressed the long $Ca_v1.3$ variant ($Ca_v1.3_L$) to test if 43S RNA can be artificially derived from a 43L template. Fig. 1*b* shows that neither cDNA isolated from transfected tsA-201 cells nor cloned PCR fragments containing exon 43L gave rise to 43S bands. Relative quantitative assessment of RNA expression was investigated either with quantitative PCR using TaqMan Gene Expression assays (Applied Biosystems) or with transcript scanning (14). For calculations of absolute copy numbers in quantitative PCR, slope values of the assays for exon 42 (Mm00551393_m1), 42A (15), 49 (Mm01209927_g1), and GAPDH (Mm99999915_g1) were obtained from standard curve experiments with assay-specific standard DNA fragments as published (12, 15). Slope, elevation, and intercepts

of standard curves for exon 42 and exon 49 probes were not significantly different. For normalization to GAPDH transcript abundance, the slopes were confirmed to show no significant statistical differences in whole brain samples (Graphpad Prism 5.0, Graphpad Software, San Diego, CA), and an average slope value (−3.43 for ventral tegmental area, −3.50 for other tissues) was derived for normalization. All samples were measured in triplicates. Samples without template and samples containing 20 ng of RNA served as negative controls.

Quantification of the different splice forms $Ca_v1.3_{43S}$ and $Ca_v1.3_{43L}$ by transcript scanning was based on published methodology (16). Exon-spanning primers 5′-CGAGCCAGAAGACTCCAAA-3′ (forward) and 5′-CACAGCACTCCTCGCTACTG-3′ (reverse) were used in PCR (95 °C for 5 min, 30 cycles of 92 °C for 30 s, 58 °C for 30 s, 72 °C for 1 min) with 50 ng of mouse whole brain or 100 ng of mouse whole heart RNA equivalents as templates. PCR was performed using PCR Master Mix (Fermentas) and produced two fragments of distinct size (~400 and ~550 bp). The PCR products were extracted from 1% agarose gels using the NucleoSpin Kit (Macherey-Nagel), ligated with the pJET1.2/blunt vector (Clone JET PCR Cloning Kit, Fermentas), and replicated in DH5α cells. Resulting clones were analyzed with colony PCR (95 °C for 3 min, 30 cycles of 94 °C for 30 s, 60 °C for 30 s, 72 °C for 1 min) using primers flanking the multiple cloning site of the vector (forward, 5′-CGACTCACTATAGGGAGAGCGGC-3′; reverse, 5′-AAGAACATCGATTTTCCATGGCAG-3′). PCR products containing 43S or 43L were distinguished on 1.5% agarose gels and verified by sequencing of the representative extracted fragments. The assay slightly overestimated the presence of the short variant as determined using fixed ratios of cDNA templates containing exon 43S ($Ca_v1.3_{43S}$ α1) and 43L ($Ca_v1.3_L$ α1): 43S/43L ratio added, 0.10, measured 0.14 ($n = 116$); ratio added 0.50, measured 0.69 ($n = 172$). This indicated an overestimation of 38–40% of the short form, and the data were corrected accordingly.

Cloning of Expression Constructs

For the $Ca_v1.3_{43S}$ splice variant, a 1217-bp fragment was generated by PCR with primers 5′-TCGGCAGCATTATAGACGTG-3′, 5′-ATAGGATCCCTATGGAATTATGGTTATGATGGTTATGACACACCGAATTTCCTGTTTGAACACATCATCTTCTTCTTC-3′, and human $Ca_v1.3_L$ cDNA expression construct as template (GenBank accession number EU363339). The PCR product was incorporated into the same construct after the HindIII/BamHI digest. $Ca_v1.2$ α1 cDNA (GenBank accession number X15539) was used to generate a N-terminal GFP-labeled $Ca_V1.2_{C349}$ C-terminal peptide (GFP-$Ca_v1.2_{C349}$). A fragment flanked by artificially introduced EcoRI and HindIII restriction sites was generated by PCR (forward primer, 5′-AAG CTT GAG GGC CAC GGG TCC CC-3′; reverse primer, 5′-GAA TTC CTA CAG GCT GCT GAC GCC-3′) and subsequently ligated with vector $pGFP^+$ (17) to generate $Ca_v1.2$ peptide 1821–2175 in the N-terminal fusion with GFP cDNA. For all expression constructs, regions subjected to PCR were confirmed by sequencing (MWG). Cloning of construct GFP-$Ca_v1.3_{C158}$ has been described (8).

Cell Culture and Transfection

For whole cell patch clamp recordings, tsA-201 cells (a human embryonic kidney cell line stably expressing a SV40 temperature sensitive T antigen, ECACC, number 96121229) were cultured in Dulbecco's modified Eagle's medium (DMEM) supplemented with 10% fetal bovine serum (Invitrogen, 10270–106), 2 mM glutamine (Invitrogen, 25030-032), penicillin (10 units/ml; Sigma, P-3032), and streptomycin (10 μg/ml; Sigma, S-6501) and maintained at 37 °C in a humidified incubator with 10% CO_2. Cells were grown and split when they reached about 80% of confluence using 0.05% trypsin for cell dissociation. Cell passage numbers did not exceed 20 passages. For whole cell patch clamp recordings tsA-201 cells were transiently transfected using Ca^{2+}-phosphate as described previously (8) with an equimolar ratio of cDNA encoding full-length $Ca_v1.3_L$, $Ca_v1.3_{42A}$, or $Ca_v1.3_{43S}$ α1-subunits together with auxiliary $Ca_v\beta3$ and $Ca_v\alpha2\delta1$ subunits (8). Note that full-length human $Ca_v1.3_L$ channels are identical to $Ca_v1.3_{42}$ and $Ca_v1.3_{8A}$ channels (GenBank™ accession number EU363339) reported in our previous publications (8, 18) but nomenclature has now been changed for clarity. To visualize transfected cells either GFP alone or N-terminal GFP-labeled constructs were used. Cells were then plated onto a 35-mm culture dish containing poly-L-lysine-precoated coverslips. The cells were kept at 30 °C and 10% CO_2, and subjected to electrophysiological measurements 18 h after transfection.

For single channel recordings, HEK-293 cells were cultured in Petri dishes in Dulbecco's modified Eagle's medium (DMEM; PAA, Pasching, Austria) supplemented with 10% FBS (Sigma), penicillin (10 units/ml), and streptomycin (10 μg/ml) (Sigma). Cells were routinely passaged twice a week and incubated at 37 °C under 6% CO_2. For transient transfection, HEK-293 cells were seeded onto 60-mm polystyrene Petri dishes (Falcon, Heidelberg, Germany) at a density of $1–2 \times 10^4$ cells/cm^2. The amount of $Ca_v1.3_L$, $Ca_v1.3_{42A}$ or $Ca_v1.3_{43S}$ α_1, $Ca_v\beta_3$, $Ca_v\alpha_1\delta1$, and GFP cDNA transfected was 2, 1, 1.5, and 0.5 μg, respectively. The cDNA mixture was delivered to HEK-293 cells by Effectene® transfection (Qiagen) according to the manufacturer's guidelines. 16–20 h after transfection, cells were split and cultured in 35-mm polystyrene Petri dishes (Falcon, Heidelberg, Germany) under the normal growth conditions.

Electrophysiological Recordings

Whole Cell Patch Clamp Recordings—Electrodes with a resistance of 2–5 megaohms were pulled from glass capillaries (Borosilicate glass, 64–0792, Harvard Apparatus) using a micropipette puller (Sutter Instruments) and fire-polished with an MF-830 microforge (Narishige, Japan). Cells were recorded in the whole cell configuration using Axopatch 200A amplifier (Axon Instruments, Foster City, CA). Data were analyzed using pClamp 9 software. The pipette internal solution contained (in mM): 135 CsCl, 10 HEPES, 10 Cs-EGTA, 1 $MgCl_2$ adjusted to pH 7.4 with CsOH (311 mosmol); bath solution: 15 $CaCl_2$, 10 HEPES, 150 choline-Cl, and 1 $MgCl_2$, adjusted to pH 7.4 with CsOH (320 mosmol). Current-voltage (*I-V*) relationships were obtained by holding cells at a potential of −80 mV (holding potential, HP) before applying 250-ms pulses to various test

potentials. *I-V* curves were fitted to the equation $I = G_{max}(V - V_{rev})/\{1 + \exp[(V - V_{0.5act})/k]\}$, where V_{rev} is the extrapolated reversal potential, V is the test potential, I is the peak current amplitude, G_{max} is the maximum slope conductance, $V_{0.5,act}$ is the half-maximal activation voltage, and k is the slope factor. Percentage of inactivation was determined at specified time points during depolarizing pulses from a HP of −80 mV to the peak current potential (V_{max}) of the *I-V* relationship of the individual cell. The voltage dependence of inactivation was assessed by application of a 20-ms test pulse to V_{max} before and after holding cells at various conditioning test potentials for 5-s. Steady-state inactivation curves were analyzed using the following Boltzman relationship: $I = I_{SS} + (1 - I_{SS})/(1 + \exp(V - V_{0.5,inact}/k_{inact}))$, where I is the peak current amplitude, I_{ss} is the noninactivating fraction, V is the membrane potential, $V_{0.5,inact}$ is the half-inactivation potential, and k_{inact} is the slope factor. Experiments showing currents bigger than 3 nA were prospectively excluded from analysis of activation and inactivation parameters to guarantee high-quality voltage clamp. CDI was quantified as the current remaining at the end of 250-ms depolarizations to different test potentials (expressed as fraction of the peak current amplitude, r_{250}). Parameter f was defined as the maximal difference between r_{250} values of the barium (I_{Ba}) and calcium (I_{Ca}) inward currents observed within the investigated voltage range. ON-gating charge (Q_{ON}) was measured by holding the cells at −80 mV before applying a 20-ms test pulse to V_{rev} where no net inward current was observed. ON-gating currents were digitized at 50 kHz and filtered at 5 kHz and quantified by current integration over the first 2 ms of the test pulse.

Action potential waveform (APW)-like stimulus trains were applied as ramp steps (see Fig. 8). Leak potentials and capacitive transients were subtracted after blocking the current by 0.5 mM Cd^{2+}, 0.2 mM La^{3+}. APWs were applied 50 times at frequencies of 100, 25, and 5 Hz resulting in 10-, 40-, and 200-ms trains, respectively. Ca^{2+} influx was quantified by integration of the first 80 (at 100 Hz), 320 (at 25 Hz), and 1600 ms (at 5 Hz) of I_{Ca} train activity. Percentage of inactivation during train stimulation was determined by the ratio between the first and the 8th I_{Ca} amplitude. Recovery of inactivation was measured during a 10-ms test pulse to V_{max} that were applied at various durations after a 1-s voltage prepulse to V_{max}. The time course of recovery was fit to mono- or biexponential decay yielding time constants for the fast (τ_{fast}) and slow (τ_{slow}) component. The interpulse interval was 10-s. Linear leak and capacitative currents were subtracted online with a P/4 protocol. All voltages were corrected for the liquid junction potential of 8.5 (for 15 mM Ca^{2+}) or 9 mV (for 2 mM Ca^{2+}). Series resistance was compensated at 60–70%. All experiments were performed at room temperature (~25 °C).

Single Channel Patch Clamp Recordings—Single channel currents through $Ca_v1.3$ channel splice variants in GFP-positive cells were obtained 48–72 h after transfection. Recording and analysis were performed at room temperature (19–23 °C) as reported (19, 20). In brief, cells kept in 35-mm culture dishes were washed and placed in a depolarizing bath solution containing (in mM) 120 potassium glutamate, 25 KCl, 2 $MgCl_2$, 10 HEPES, 2 EGTA, 1 $CaCl_2$, 1 Na_2ATP, 10 dextrose (pH 7.4 with KOH). Patch pipettes made from borosilicate glass (1.7-mm diameter and 0.283-mm wall thickness, Hilgenberg GmbH, Malsfeld, Germany) were pulled using a Narishige PP-83 vertical puller and fire-polished using a Narishige MF-83 microforge (Narishige Scientific Instrument Lab). Pipettes showed typical resistances between 7 and 10 megaohm when filled with pipette solution (in mM), 15 $BaCl_2$, 105 triethanolamine-Cl, 10 HEPES (pH 7.4 with triethanolamine-OH). Single Ca^{2+} channels were recorded in the cell-attached configuration at test potentials ranging from −30 to 0 mV and depolarizing test pulses of 150-ms duration at 1.67 Hz (HP −100 mV). Single channel currents were amplified, filtered at 2 kHz, −3 decibel, 4-pole Bessel, and sampled at 10 kHz with the Axopatch one-dimensional amplifier using pClamp 5.5 software (Axon Instruments). Experiments were analyzed whenever the channel activity persisted for at least 240 sweeps for each test potential, with no stacked openings observed. The single channel events were detected using pClamp 6.0 software (Axon Instruments), and Origin 5 software (Microcal Software, Northampton, MA) was employed for graphic analysis. Single channel gating analysis was performed as described (20). To determine unitary conductance of $Ca_v1.3$ channels, single channel amplitude was determine from all point histograms by fitting two Gaussians. Single channel conductance was calculated as the slope of the current-voltage relationship.

Statistics

All values are presented as mean ± S.E. for the indicated number of experiments (n). For multiple comparisons statistical significance was determined by one-way analysis of variance (ANOVA) followed by Bonferroni multiple comparison or Dunnett's post hoc test. For comparisons of two groups, data were analyzed by a Mann-Whitney test as indicated for individual experiments. Statistical significance was set at $p < 0.05$.

RESULTS

Identification and Expression of Novel C Terminally Spliced $Ca_v1.3$ LTCCs—Based on our previous finding that alternative splicing within the C terminus alters Ca^{2+} influx through $Ca_v1.3$ LTCCs, we investigated if further unknown C-terminal splice variants exist. So far, exon 42 was believed to participate only in the formation of functionally "long" $Ca_v1.3$ variants (*i.e.* containing both, the PCRD encoded by exon 42 and the DCRD encoded by exon 49; $Ca_v1.3_L$, Fig. 1*a*), which implied that transcripts derived from exons 42 and 49 would occur with similar abundances. However, this was not the case when we applied a quantitative PCR approach with samples from different mouse brain regions. The relative abundance of exon 42 exceeded the abundance of exon 49 in all brain regions tested (Fig. 1*b*). This finding suggested the presence of a substantial amount of transcripts containing exon 42 but not exon 49, likely due to an additional alternative splicing event between exons 42 and 49. With PCR primers spanning exons 42 to 45 we indeed identified a novel splice variant that resulted from the use of an alternative 3′ splice acceptor site, causing a shortening of exon 43 (thus termed exon 43S; Fig. 1*a*). mRNA containing 43S was detected in human (Fig. 2*a*) and mouse brain (Fig. 2*b*). The alternative splicing event causes a frameshift that produces a shorter C terminus and an additional unique 15-amino acid

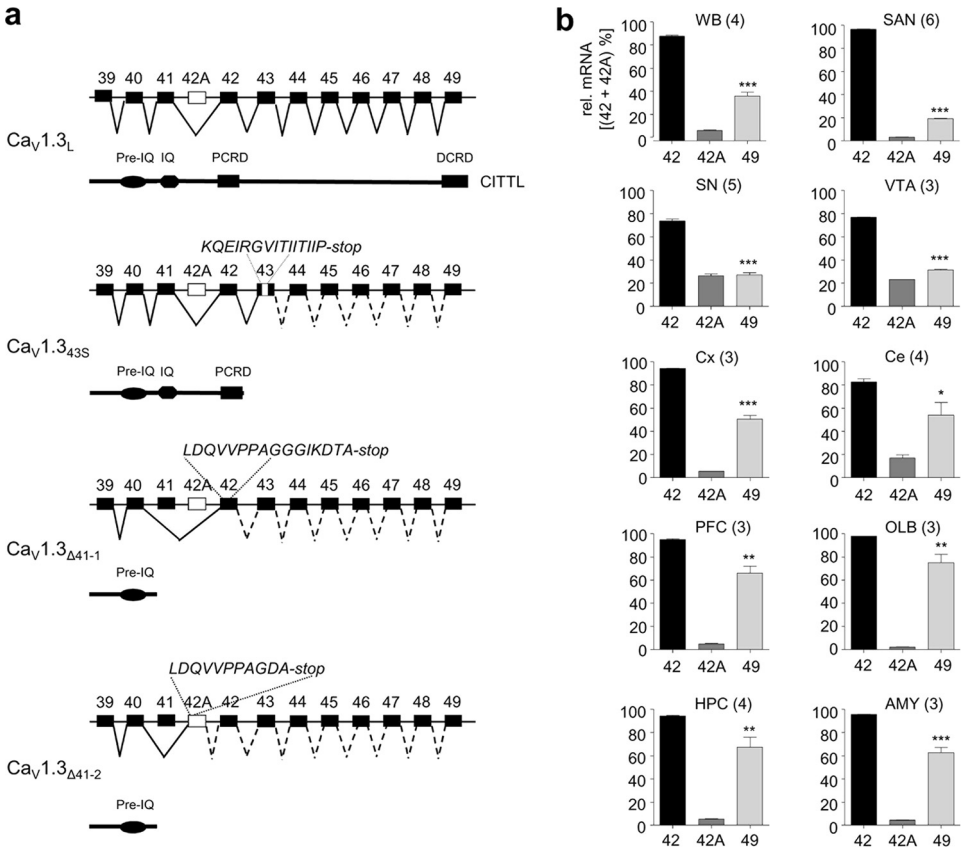

FIGURE 1. **C-terminal regulatory domains and quantitative PCR using TaqMan gene expression assays.** *a*, schematic presentation of alternative splicing in the C terminus of $Ca_v1.3$ channels generating multiple $Ca_v1.3$ $\alpha1$ isoforms with different C-terminal lengths. Constitutive and alternative exons are shown as *black* and *white squares*, respectively. The schematic protein domain structure is always shown below. $Ca_v1.3_L$, expression of exons 39 to 49 (with/without exon 44 (8)) yields the full-length $Ca_v1.3$ C terminus. $Ca_v1.3_{43S}$, use of an alternative 3′ splice acceptor site in exon 43 yields a C-terminal truncated $Ca_v1.3$ splice variant that terminates in the amino acid sequence, *KQEIRGVITIITIIP*. $Ca_v1.3_{\Delta41-1}$, $Ca_v1.3_{\Delta41-1}$ channels arise from skipping exon 41 and combining with exon 42 (terminating with *LDQVVPPAGGGIKDTA*). $Ca_v1.3_{\Delta41-2}$ combined with exon 42A (terminating with *LDQVVPPAGDA*). *b*, relative comparison of transcripts containing exon 42 (42, *black*), exon 42A (42A, *dark gray*), and exon 49 (49, *light gray*) in brain and heart regions of WT c57Bl6/N mice. Expression in percent (mean ± S.E.) relative to the sum of 42 and 42A transcripts was detected in 5 whole brains (*WB*), 20 ng (all others) of RNA equivalent from individuals (WB) or tissue pools (all others; 10 animals) are indicated. The number of experiments is given in *parentheses*. Statistical analysis was performed using one-way ANOVA followed by Bonferroni post hoc testing; *, $p < 0.05$; **, $p < 0.01$; ***, $p < 0.001$, 42 *versus* 49. *VTA*, ventral tegmental area; *Cx*, cortex; *Ce*, cerebellum; *PFC*, prefrontal cortex; *OLB*, olfactory bulb; *HPC*, hippocampus; *AMY*, amygdala.

C-terminal sequence (Fig. 1*a*). 43S was abundant in different brain areas but only very weakly expressed in the heart including the sinoatrial node (SAN) (Fig. 2*c*). As outlined in detail under "Experimental Procedures" we could rule out that exon 43S PCR products were artificial transcripts (Fig. 2*c*).

Unfortunately, no selective probes for quantitative real time PCR could be obtained for 43S (not shown). We therefore applied transcript scanning as an alternative method of quantification (14). Transcripts containing short and long exon 43, respectively, were amplified from whole brain and heart and the relative abundance of these splice variants was determined by colony PCR (see "Experimental Procedures"). In whole brain tissue, $Ca_v1.3_{43S}$ variants represented 39 ± 7% ($n = 195$) of the clones, suggesting that $Ca_v1.3_{43S}$ $\alpha1$ subunits account for a large proportion of $Ca_v1.3$ $\alpha1$ brain transcripts.

$Ca_v1.3$-mediated Ca^{2+} influx has recently been implicated in the selective vulnerability of dopaminergic SNc neurons observed in Parkinson disease (21, 22). Both short variants, $Ca_v1.3_{43S}$ (Fig. 2*b*) and $Ca_v1.3_{42A}$ (Fig. 1*b*), were expressed in the substantia nigra (SN) and the adjacent ventral tegmental area. Interestingly, in real time PCR experiments 42A-containing transcripts were more abundant in the SN and ventral tegmental area than in other brain areas (Fig. 1*b*).

A much lower percentage of 43S was found in the heart (6 ± 1%, $n = 213$). These semiquantitative estimates of the relative abundance of exon 43S as compared with 43L are in good agreement with the relative abundance of the respective PCR bands on agarose gels (Fig. 2, *b* and *c*). In SAN, the predominant site of $Ca_v1.3$ expression in the heart, 43S abundance was comparable with whole heart and all other heart regions tested (Fig. 2*c*).

Our PCR screen also revealed splice variants in human brain lacking exon 41 with exon 40 either connected to exon 42 or 42A ($\Delta41_1$ and $\Delta41_2$, Figs. 1*a* and 2*d*). Using selective *in situ* hybridization probes for $Ca_v1.3_{42A}$ and $Ca_v1.3_L$ together with a generic $Ca_v1.3$ probe we found no major differences in the expression pattern of these two isoforms in mouse brain. This is illustrated for hippocampus, olfactory bulb, and cerebellum in supplemental Fig. S1 but was also true for other brain areas, such as the cerebral cortex and caudate putamen ($n = 3$, not illustrated).

$Ca_v1.3_{43S}$ Channels Show "Short" Gating Properties—As illustrated in Fig. 1*a*, alternative splicing in exon 43 creates a

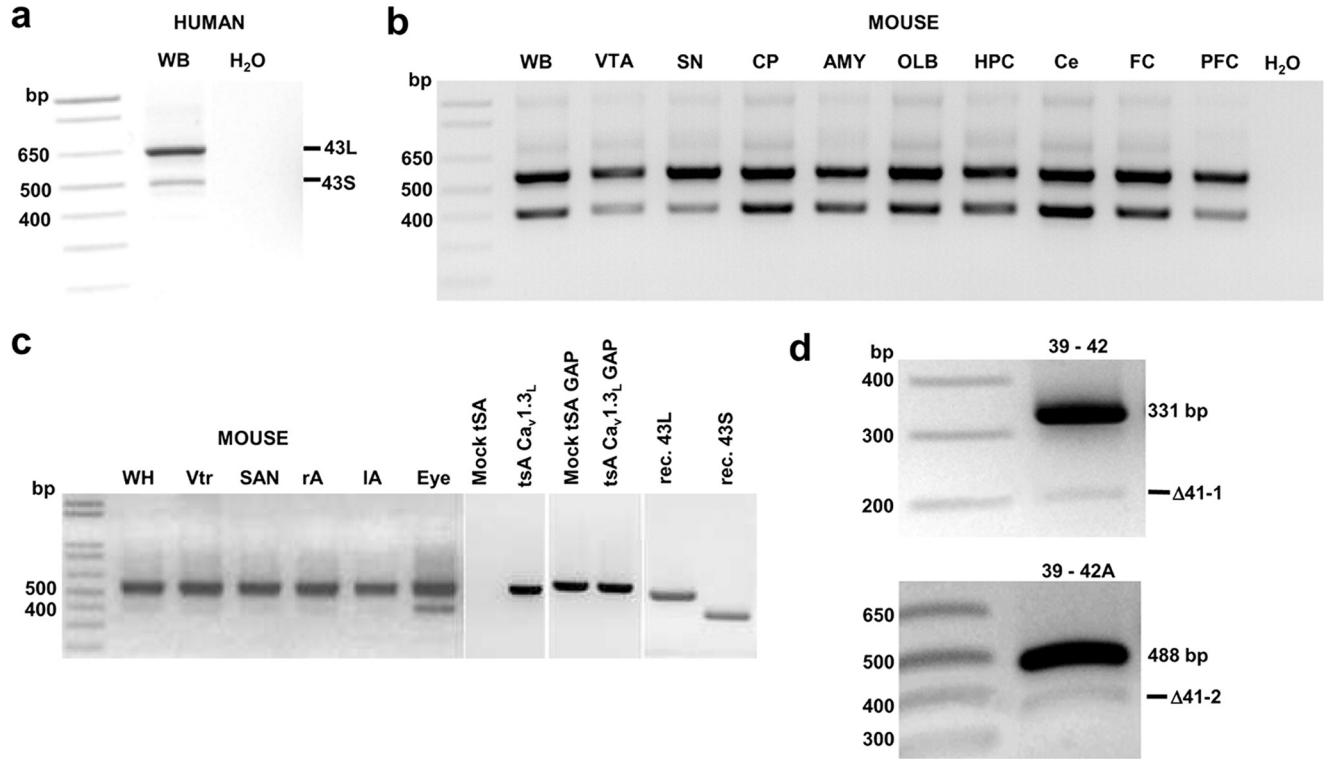

FIGURE 2. **Detection by PCR of the C-terminal alternative splicing in human and mouse $Ca_v1.3$ transcripts.** *a,* fragments containing exon 43S (502 bp) or 43l (656 bp) generated by primers specific for exon 39 (forward) and 43 (reverse) of human $Ca_v1.3$. *WB*, 500 ng of whole brain cDNA (positive control); H_2O, no template (negative control). One representative of 4 experiments is shown. *b,* fragments containing 43S (403 bp) or 43L (557 bp) were generated by primers specific for exons 42 (forward) and 45 (reverse) of mouse $Ca_v1.3$. Each sample contained 20 ng of RNA equivalent. *VTA*, ventral tegmental area; *CP*, caudate putamen; *AMY*, amygdale; *OLB*, olfactory bulb; *HPC*, hippocampus; *Ce*, cerebellum; *FC*, frontal cortex; *PFC*, prefrontal cortex. One representative of 3 experiments is shown. *c*, conditions are as described in *b*. *WH*, whole heart; *Vtr*, ventricle; *rA*, right atrium; *lA*, left atrium; *Eye*, whole eye preparation; *Mock tsA*, untransfected tsA-201 cells; *tsA $Ca_v1.3_L$*, tsA-201 cells transiently expressing mouse $Ca_v1.3_L$; all samples were tested for GAPDH expression and contamination. *GAP*, PCR with primers specific for human GAPDH. One representative of 3 experiments is shown. *d,* fragments containing exons 41 (39–42, 331 bp; 39–42A, 488 bp), Δ41–1 (39–42, 200 bp), or Δ41–2 (39–42A, 357 bp) generated by primers specific for exon 39 and exons 42 or 42A, respectively, of human $Ca_v1.3$. 1 μg of whole brain cDNA was used. One representative of 6 independent experiments is shown.

short variant that, in contrast to $Ca_v1.3_{42A}$, retains the proximal part (PCRD) of the CTM. We therefore tested if this difference distinguished the biophysical properties of $Ca_v1.3_{43S}$ from those of $Ca_v1.3_{42A}$ channels when expressed under identical experimental conditions in tsA-201 cells. As expected, with 15 mM Ca^{2+} (or Ba^{2+}) as charge carrier, $Ca_v1.3_{43S}$ resembled a short $Ca_v1.3$ channel lacking a functional CTM (Fig. 3, Table 1). I_{Ca} through $Ca_v1.3_{43S}$ channels activated and inactivated at more negative voltages than $Ca_v1.3_L$ (Fig. 3, *a* and *b*). Moreover, CDI (defined as the difference between the extent of inactivation of I_{Ba} *versus* I_{Ca}) was significantly more pronounced (Fig. 3, *c* and *d*), whereas voltage-dependent inactivation (defined as inactivation in equimolar Ba^{2+}) was slower (see I_{Ba} after 250 ms, *e.g.* −11.5 mV in Fig. 3*c*). Maximal CDI essentially was as reported for $Ca_v1.3_{42A}$ ($f = 0.6$ with a maximum at +10 mV (8)). A more negative activation range for $Ca_v1.3_{43S}$ was also found for I_{Ba} as charge carrier ($V_{0.5,act}$ (in mV): $Ca_v1.3_L$, −13.8 ± 1.6, $n = 9$; $Ca_v1.3_{43S}$, −26.01 ± 2.5, $n = 8$, $p < 0.001$, Mann-Whitney test). Because the biophysical parameters obtained were very similar to those already described by us for $Ca_v1.3_{42A}$ (8) the presence of the PCRD apparently did not affect the gating properties under these experimental conditions.

Alternative Splicing Affects Channel Open Probability—We have previously found that the absence of a functional CTM in $Ca_v1.3_{42A}$ also decreased the ratio of ON-charge movement (Q_{ON}, reflecting the capacitative voltage sensor movements upon depolarization during channel gating) to ionic tail current amplitude, which can both be measured using a single pulse protocol (Fig. 4*a*). Whereas ionic current through $Ca_v1.3_L$ was always preceded by a measurable gating current (Fig. 4*a*), the majority of cells with robust I_{Ca} through $Ca_v1.3_{43S}$ (9 of 20) and $Ca_v1.3_{42A}$ (9 of 20) did not reveal any detectable Q_{ON} (not illustrated). In cells with measurable Q_{ON} (shown in Fig. 4), mean Q_{ON} was also significantly smaller for both short variants as compared with $Ca_v1.3_L$ ($p < 0.001$ Mann-Whitney test; Fig. 4, *a* and *b*) and this was seen over a wide range of corresponding tail current amplitudes (Fig. 4*c*). This effect was also obvious from the 5–10-fold increase of the slope of the I_{Ca}-Q_{ON} relationship seen in short channels (Fig. 4*c*). These data indicate that both short isoforms possess a higher open probability (P_{open}) once the voltage sensors have opened the channel, or a higher single channel conductance. However, another interpretation is that the CTM immobilizes a component of the gating current that is not required for pore opening (thereby decreasing Q_{ON}). We therefore performed single channel analysis to directly determine the effects of C-terminal splicing on single channel behavior.

Loss of C-terminal Modulation in $Ca_v1.3$ LTCCs Increases Single Channel Activity—On the single channel level, changes in channel activity can be due to differences in the number of

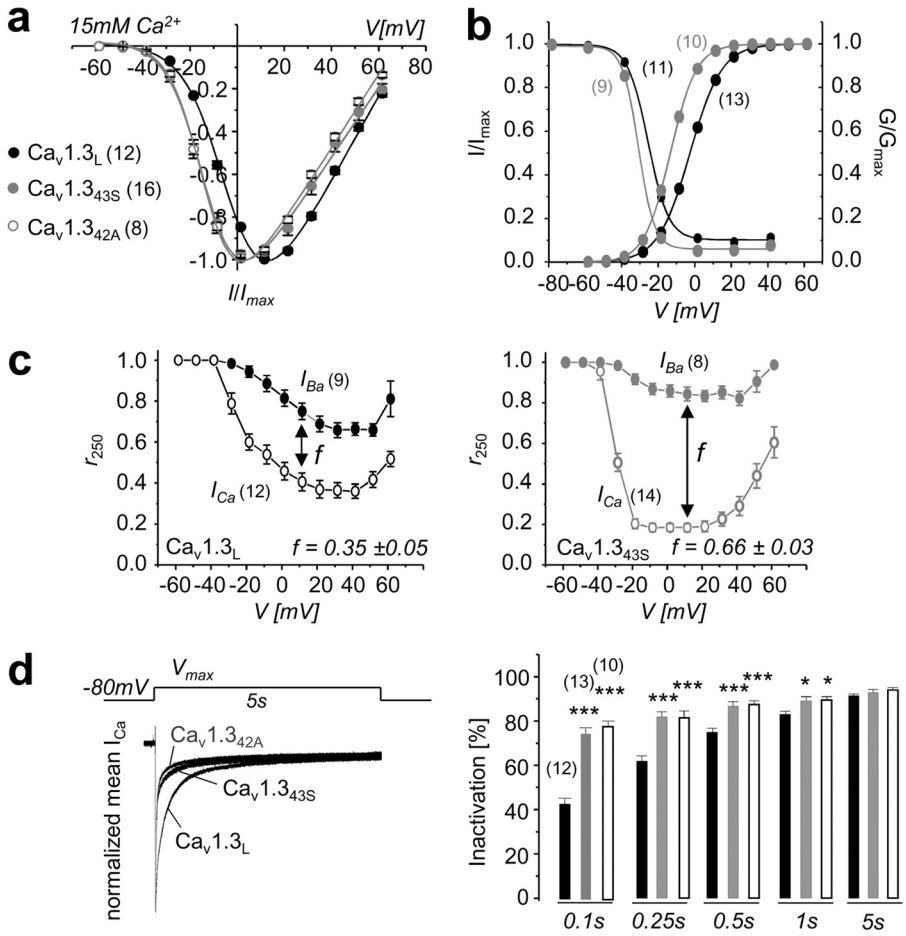

FIGURE 3. **Biophysical properties of C-terminal $Ca_v1.3$ α1 splice variants with 15 mM Ca^{2+} as charge carrier.** *a,* mean normalized current-voltage (*I-V*) curves recorded in tsA-201 cells expressing $Ca_v1.3_L$ (*black*), $Ca_v1.3_{43S}$ (*open circle*), and $Ca_v1.3_{42A}$ (*gray*). Activation parameters and statistics are given in Table 1. *b,* steady-state inactivation curves for $Ca_v1.3_L$, $Ca_v1.3_{43S}$. Parameters for the activation curve were obtained from parameters in *a*. Inactivation parameters were as follows in mV: $V_{0.5}$, $Ca_v1.3_L$, -25.6 ± 0.52; $Ca_v1.3_{43S}$, -30.9 ± 0.7, $p < 0.001$; *k* (slope): $Ca_v1.3_L$, -5.5 ± 0.26, $Ca_v1.3_{43S}$, -4.2 ± 0.2, $p = 0.027$, Mann-Whitney test. *c,* voltage dependence of CDI for $Ca_v1.3_L$ (*left*) and $Ca_v1.3_{43S}$ (*right*): r_{250} corresponds to the fraction of I_{Ca} or I_{Ba} remaining after 250 ms; *f* is the difference between r_{250} values at 11.5 mV. *d, left*, normalized peak current traces of $Ca_v1.3_L$, $Ca_v1.3_{43S}$, and $Ca_v1.3_{42A}$ evoked by 5-s depolarization to V_{max}. *Right*, percent I_{Ca} inactivation during 0.1-, 0.25-, 0.5-, 1-, and 5-s test pulses to V_{max}. Color code as described in *a*. Number of experiments is given in *parentheses*. *Error bars* reflect S.E. *, $p < 0.05$; ***, $p < 0.001$, one-way ANOVA analysis followed by Bonferroni post test.

TABLE 1

Biophysical properties of $Ca_v1.3$ α1 splice variants with 15 mM Ca^{2+} as charge carrier

Channel	$V_{0.5,act}$	Slope	V_{max}	V_{rev}	Activation threshold	*n*
			mV			
$Ca_v1.3_L$	-2.4 ± 0.6	$-8.6 + 0.2$	$12.6 + 0.5$	71.9 ± 1.0	-32.6 ± 0.3	13
$Ca_v1.3_{43S}$	-13.0 ± 0.7^a	-6.9 ± 0.2^a	1.7 ± 0.8^a	68.6 ± 0.7	-35.5 ± 0.6^b	16
$Ca_v1.3_{42A}$	-12.1 ± 1.6^a	-7.5 ± 0.5^c	0.6 ± 3.5^a	75.9 ± 1.4	-32.0 ± 1.0^a	8
$Ca_v1.3_{43S} + 1.3_{C158}$	-0.09 ± 1.6^d	-9.0 ± 0.3^d	14.6 ± 1.6^d	70.7 ± 2.4	-32.1 ± 1.1^e	9
$Ca_v1.3_{43S} + 1.2_{C349}$	1.4 ± 1.3^d	-9.6 ± 0.2^d	16.6 ± 1.3^d	74.0 ± 1.4^e	-33.0 ± 0.9^e	12

[a] $p < 0.001$, comparison with $Ca_v1.3_L$. One-way ANOVA was followed by Bonferroni post test.
[b] $p < 0.01$, comparison with $Ca_v1.3_L$. One-way ANOVA was followed by Bonferroni post test.
[c] $p < 0.05$,comparison with $Ca_v1.3_L$. One-way ANOVA was followed by Bonferroni post test.
[d] $p < 0.001$, comparison with $Ca_v1.3_{43S}$. One-way ANOVA was followed by Bonferroni post test.
[e] $p < 0.05$, comparison with $Ca_v1.3_{43S}$. One-way ANOVA was followed by Bonferroni post test.

open channels, the single channel conductance, or the probability of channel opening. To discriminate between these possibilities we performed cell-attached single channel experiments using 15 mM Ca^{2+} as charge carrier, as in our whole cell recordings. As apparent from the representative experiments in Fig. 5, P_{open} was much higher in both short forms as compared with $Ca_v1.3_L$ channels (see also supplemental Table S1). As a consequence, much larger ensemble average current amplitudes were observed for the short forms (Fig. 5, *a-c*), in good agreement with the higher slope of the I_{Ca}-Q_{ON} relationship (Fig. 4*c*) and a trend to larger current densities measured in our whole cell experiments (in pA/pF: $Ca_v1.3_L$, 22.4 ± 4.5, $n = 12$; $Ca_v1.3_{43S}$, 32.1 ± 6.5, $n = 16$; $Ca_v1.3_{42A}$, 44.6 ± 10.6, $n = 9$). P_{open} of $Ca_v1.3_{43S}$ was slightly lower than of $Ca_v1.3_{42A}$, and this difference was significant at −30 and −10 mV. Except for the most negative voltage that could be tested (−30 mV) the fraction of active sweeps was comparable (Fig. 5*e*). Single channel currents mediated by $Ca_v1.3_{43S}$ and $Ca_v1.3_{42A}$ α1 subunits were

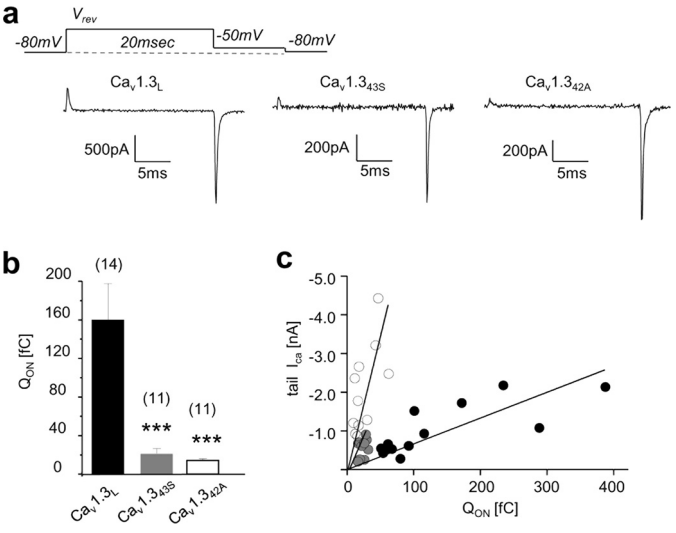

FIGURE 4. **Differential coupling of ON-gating current to the opening of $Ca_v1.3$ splice variant α1-subunits at the reversal potential.** *a*, ON-gating currents were measured at potentials at which no ionic inward and outward current was observed (V_{rev}). V_{rev} was determined individually in each cell by 20-ms pulses to voltages between +70 and +90 mV in 2-mV increments. Tail current was elicited during repolarization to −50 mV as indicated in the step protocol above. Representative currents are shown below (cells: $Ca_v1.3_L$, 091009_62; $Ca_v1.3_{43S}$, 081009_96; $Ca_v1.3_{42A}$, 151009_15). *b*, *bar graphs* show ON-gating current (Q_{ON}) for $Ca_v1.3_L$ (*black*), $Ca_v1.3_{43S}$ (*gray*), and $Ca_v1.3_{42A}$ (*white*). *Error bars* reflect S.E. ***, $p < 0.001$ (Mann-Whitney test). Number of experiments is given in *parenthesis*. *c*, correlation of Q_{ON} to maximal tail current amplitude at V_{rev}. Color code according to *b*. Calculated slopes were: −0.0067 ± 0.0008 for $Ca_v1.3_L$, −0.0403 ± 0.0005 for $Ca_v1.3_{43S}$, and −0.0705 ± 0.012 for $Ca_v1.3_{42A}$, respectively.

slightly, but not significantly lower compared with $Ca_v1.3_L$ (Fig. 5*f*).

Distinct Gating Properties of the Two Short Splice Forms at Physiological Ca^{2+} Concentrations—Because $Ca_v1.3_{43S}$, but not $Ca_v1.3_{42A}$, still contains the PCRD domain of the CTM, which is located in close proximity to the CaM binding site, we hypothesized that functional differences may be revealed at lower extracellular Ca^{2+} concentrations. We therefore also studied the properties of all $Ca_v1.3$ variants using physiological (2 mM) extracellular Ca^{2+} in the bath solution. As expected from known surface charge screening effects (23) activation of all splice variants occurred at more negative voltages. As for higher extracellular Ca^{2+}, the short variants activated with significantly more negative $V_{0.5,act}$ values (Fig. 6*a*, Table 2). The negative shift in the voltage dependence of inactivation of the two short variants was smaller than with 15 mM Ca^{2+} and the difference to $Ca_v1.3_L$ was not statistically significant (Fig. 6*b*). Interestingly, I_{Ca} through $Ca_v1.3_{43S}$ inactivated slower than $Ca_v1.3_{42A}$ during the first 250 ms (Fig. 6*c*). The effect was also obvious from the voltage dependence of CDI. Remaining I_{Ca} at −20 mV (voltage of maximal difference of CDI) was significantly larger for $Ca_v1.3_{43S}$ than for $Ca_v1.3_{42A}$ ($Ca_v1.3_{43S}$, 0.30 ± 0.04; $Ca_v1.3_{42A}$, 0.19 ± 0.05; $p = 0.04$; Mann-Whitney test) and its *f* value was smaller (Fig. 6*d*). Our data clearly demonstrate that CDI of $Ca_v1.3$ channels differs depending on the concentration of Ca^{2+} in the bath solution and that the additional sequence downstream of the CaM interaction IQ motif also including the PCRD domain caused a small but detectable moderation of CDI in $Ca_v1.3_{43S}$ channels.

Intermolecular Modulation of $Ca_v1.3_{43S}$ Channels by a Distal C-terminal Regulatory Domain of $Ca_v1.2$ LTCCs—The presence of the PCRD domain in $Ca_v1.3_{43S}$ channels predicts another unique modulatory mechanism. We previously found that coexpression of a separate C-terminal peptide that contains the DCRD can restore a fully functional CTM with full-length channel properties in constructs lacking DCRD but still containing PCRD (8). Fig. 7 illustrates that this was also found for $Ca_v1.3_{43S}$ when coexpressed with GFP-labeled peptide 1.3_{C158} (GFP-1.3_{C158}), which comprises the last 158 amino acid residues of $Ca_v1.3_L$ and contains the DCRD. In the presence of GFP-1.3_{C158}, $Ca_v1.3_{43S}$ channel behavior was indistinguishable from $Ca_v1.3_L$ with respect to the voltage dependence of I_{Ca} activation (Fig. 7*a*) and I_{Ca} inactivation during test pulses to V_{max} (*i.e.* CDI) (Fig. 7, *b* and *c*). Because there is no published evidence for a C-terminal post-translational proteolytic processing of $Ca_v1.3_L$ in the brain, cleaved $Ca_v1.3$ C termini may actually not exist as regulatory peptides *in vivo*. Instead, C-terminal cleaved $Ca_v1.2$ channel products were found to serve as potent noncovalently bound autoinhibitors of $Ca_v1.2$ channels (24). They were also shown to exist as separate signaling molecules that can shuttle between the nucleus and cytoplasm in an activity-dependent manner (25). As $Ca_v1.2$ and $Ca_v1.3$ are frequently expressed in the same cell *in vivo* (1), C-terminal $Ca_v1.2$ peptides could modulate $Ca_v1.3_{43S}$ channels by binding to their PCRD. To test this possibility we co-expressed a GFP-labeled peptide predicted to be derived from C-terminal cleavage of $Ca_v1.2$ (GFP-1.2_{C349}) together with $Ca_v1.3_{43S}$. GFP-1.2_{C349} fully restored both voltage-dependent activation and inactivation properties of $Ca_v1.3_L$ in $Ca_v1.3_{43S}$ (Fig. 7, for statistics, see figure legend). Taken together these data suggest a distinct physiological role of $Ca_v1.3_{43S}$ channels and define a novel functional class of $Ca_v1.3$ channel variants.

Impact of C-terminal Modulation for $Ca_v1.3$ Ca^{2+} Currents during Action Potential Waveforms—Although step depolarizations over several hundred milliseconds resemble LTCC activity during cardiac action potentials or LTCC activity in sensory cells, they fail to predict the consequences of C-terminal splicing on $Ca_v1.3$-mediated Ca^{2+} entry during trains of short APWs in neurons. We therefore elicited $Ca_v1.3$ channel activity by two different pulse protocols mimicking different neuronal activity patterns at physiological extracellular Ca^{2+} concentrations. APWs simulating a rapidly firing/bursting neuron were of short duration (5 ms) and were elicited from a negative membrane potential (−70 mV, Fig. 8, *a–c*). 100 Hz trains were included because brief high-frequency bursts also occur *in vivo* in different types of neurons (26), are used experimentally to induce L-type channel-dependent LTP (27), and were added for comparison to previously published work (28) employing $Ca_v1.3$ channels. In addition, we mimicked activity patterns of SNc neurons obtained from recordings in SNc neurons. Such were elicited from more depolarized voltages (−50 mV, Fig. 8, *d–f*) at frequencies resembling either regular autonomous pacemaker activity observed in slice recordings (5 Hz) or high frequency bursts observed *in vivo* (29). Differences in the time course of Ca^{2+} entry between splice variants already became apparent during the first action potential of the APWs elicited from −70 mV (Fig. 8*a*). When normalized to peak cur-

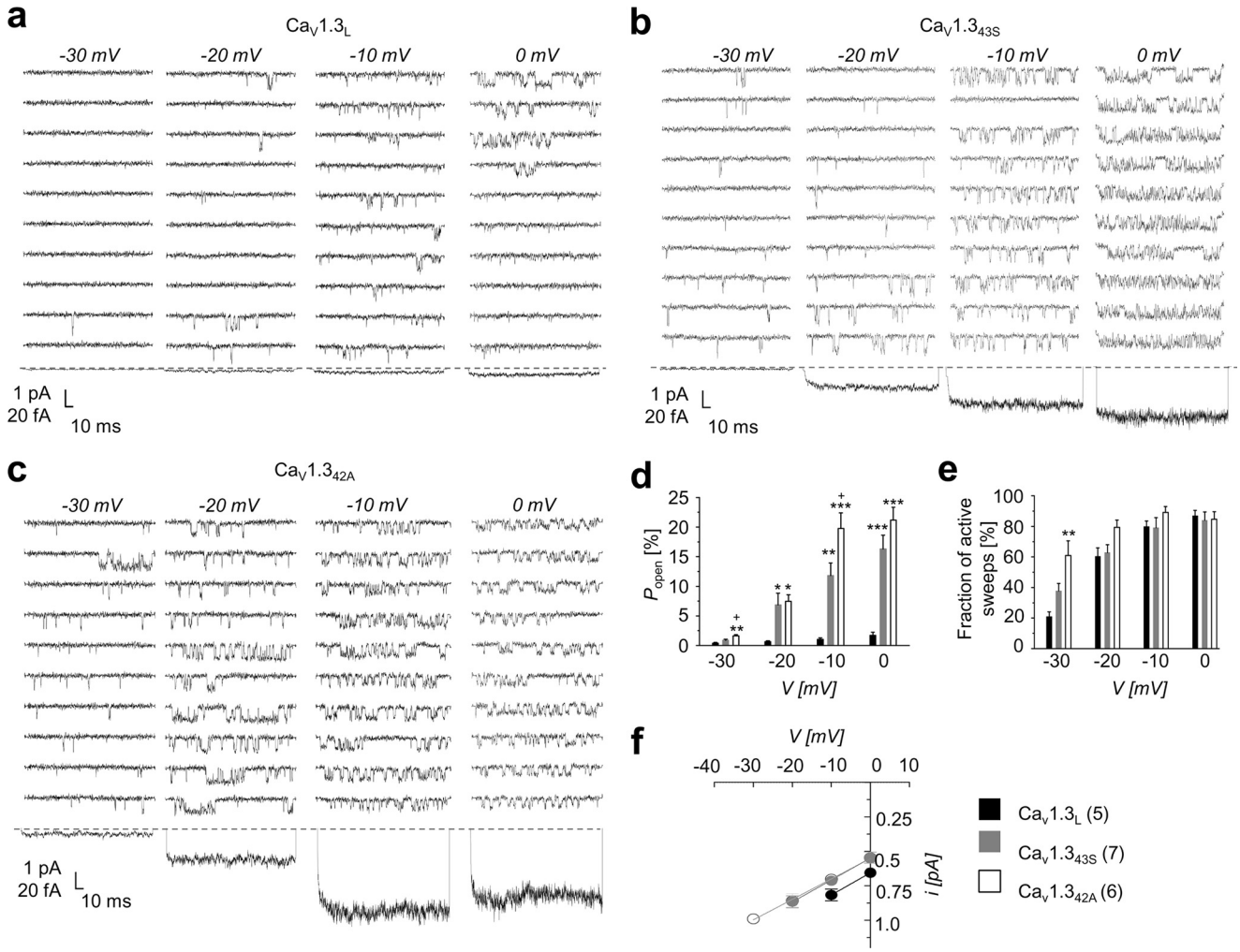

FIGURE 5. **Single channel properties of $Ca_v1.3$ C-terminal α1 subunit splice variants.** *a–c*, representative single channel recordings for $Ca_v1.3_L$, $Ca_v1.3_{42A}$, and $Ca_v1.3_{43S}$ were obtained during step depolarization to voltage ranging from −30 to 0 mV from the holding potential of −100 mV with 15 mM Ba^{2+} as the charge carrier. The depicted single channel currents were elicited by 150-ms pulses to the indicated potentials and applied every 600 ms. Ten representative consecutive traces (of at least 300 recorded traces per experiment) are depicted (cells: $Ca_v1.3_L$, C9625; $Ca_v1.3_{43S}$, J0427; $Ca_v1.3_{42A}$, I9604). Below the corresponding ensemble average current is presented. *d*, open probability (P_{open}) within active sweeps. *e*, fraction of active sweeps containing at least one channel opening. One-way ANOVA followed by Dunnett's post test was performed among all test potentials. Significance levels were: *, $p < 0.05$; **, $p < 0.01$; and ***, $p < 0.001$ for comparing with $Ca_v1.3_L$; +, $p < 0.05$ and **, $p < 0.01$ for comparison with $Ca_v1.3_{43S}$. Data are presented as mean ± S.E. *f*, current-voltage relationship of unitary currents of $Ca_v1.3_L$ (*black*, $n = 6$), $Ca_v1.3_{43S}$ (*light gray*, $n = 8$), and $Ca_v1.3_{42A}$ (*gray*, $n = 6$). *Solid line* represents the best-fit curve to data obtained from all-point histograms. Despite minor differences in unitary current level at −10 mV, single channel conductance was similar for all three isoforms (in pS: $Ca_v1.3_L$, 16.10 ± 1.97, $n = 5$; $Ca_v1.3_{43S}$, 15.94 ± 2.19, $n = 7$; and $Ca_v1.3_{42A}$, 14.86 ± 0.9, $n = 6$).

rent amplitude (I_{peak}, which occurred during the repolarization phase as tail current), short splice variants exhibited a marked early component of Ca^{2+} entry evident as a distinct peak well before the maximum of the action potential was reached (Fig. 8*a*, *left*). During repetitive stimulation, peak inward currents through all three splice variants decreased during APWs elicited from −70 mV (Fig. 8*b*), and this was already apparent during the second APW (Fig. 8*a*, *right*). During eight APWs at 100 or 25 Hz (Fig. 8*b*) twice as much peak current decayed for $Ca_v1.3_{42A}$ currents as compared with $Ca_v1.3_L$. For $Ca_v1.3_{43S}$, significantly more peak currents decayed at 100 Hz also (Fig. 8*b*, *left*). At 25 Hz, $Ca_v1.3_{43S}$ differed from $Ca_v1.3_{42A}$ ($p < 0.01$, one-way ANOVA, Bonferroni post-test, Fig. 8*b*, *right*) because the decay was indistinguishable from the long variant. Very similar differences were found for normalized I_{Ca} integrated over eight APWs (I_{Ca} area under first AP normalized to the 8th; Fig. 8*c*). During SNc-like APWs applied at 5 Hz (reflecting autonomous pacemaking), decay of I_{peak} was very small and similar for all variants (Fig. 8, *d* and *e*, *right*). In contrast, at 25 Hz (a frequency reached during short bursts recorded *in vivo* (29)), the absence of a functional CTM caused a much larger I_{peak} decay (Fig. 8*e*, *left*). This was also reflected for I_{Ca} integrated over eight stimuli (Fig. 8*f*).

The frequency-dependent larger current decay of $Ca_v1.3_{43S}$ and $Ca_v1.3_{42A}$ channels during AP trains indicates a larger accumulation of channels in inactivated states. More pronounced CDI can explain this finding. However, differences in the recovery from inactivation could be another contributing factor. As illustrated in Fig. 8*g*, $Ca_v1.3_{43S}$ and $Ca_v1.3_{42A}$ recovered more slowly than $Ca_v1.3_L$ from inactivation after a 1-s conditional prepulse. This difference was independent of the

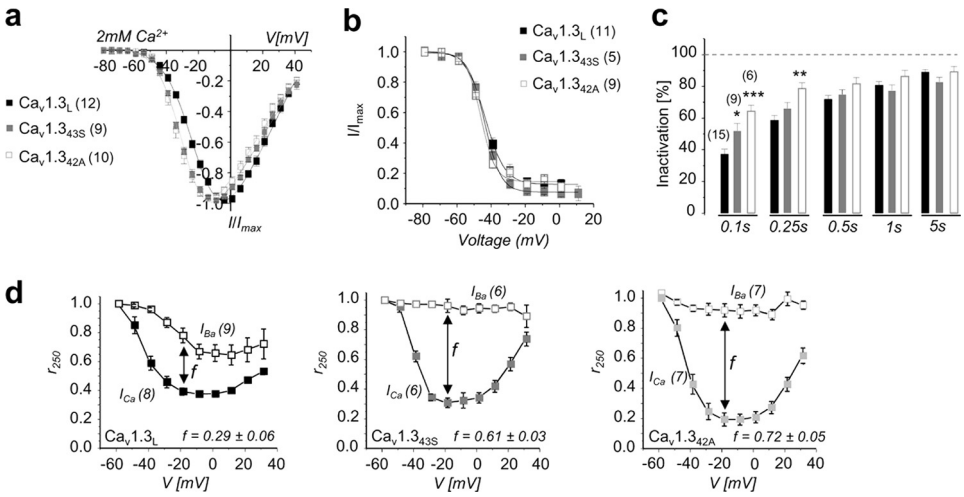

FIGURE 6. **Biophysical properties of C-terminal $Ca_v1.3$ α1 splice variants with 2 mM Ca^{2+} as charge carrier.** *a*, current activation properties shown in representative of normalized *I-V* curves recorded in tsA-201 cells expressing $Ca_v1.3_L$ (*black*), $Ca_v1.3_{43S}$ (*gray*), and $Ca_v1.3_{42A}$ (*white*). Activation parameters and statistics are given in Table 2. *b*, voltage dependence of inactivation elicited after 5-s conditioning prepulses using 20-ms test pulses to V_{max}. Inactivation parameters are given in mV: $V_{0.5,inact}$: $Ca_v1.3_L$, -43.4 ± 1.1, $Ca_v1.3_{43S}$, -43.7 ± 0.4, $Ca_v1.3_{42A}$, -46.4 ± 0.34; *k* (slope): $Ca_v1.3_L$, -5.1 ± 0.3, $Ca_v1.3_{43S}$, -4.7 ± 0.15, $Ca_v1.3_{42A}$, -4.5 ± 0.3. *c*, percent I_{Ca} inactivation during 0.1-, 0.25-, 0.5-, 1-, and 5-s test pulses to V_{max}. Color code as described in *a*. *d*, voltage dependence of CDI: r_{250} corresponds to the fraction of I_{Ca} or I_{Ba} remaining after 250 ms; *f* is the difference in r_{250} of I_{Ba} and I_{Ca} at -19 mV. Number of experiments are given in *parentheses*. *Error bars* reflect S.E. *, $p < 0.05$; **, $p < 0.01$; ***, $p < 0.001$, one-way ANOVA followed by Bonferroni post test.

TABLE 2

Biophysical properties of $Ca_v1.3$ α1 splice variants with 2 mM Ca^{2+} as charge carrier

Channel	$V_{0.5,act}$	Slope	V_{max}	V_{rev}	Activation threshold	*n*
			mV			
$Ca_v1.3_L$	-20.5 ± 1.1	-8.1 ± 0.4	-5.0 ± 1.3	55.1 ± 0.9	-49.0 ± 0.7	12
$Ca_v1.3_{43S}$	-28.6 ± 0.4^a	-6.9 ± 0.2^{ba}	-13.0 ± 0.5^a	59.9 ± 2.1	-51.4 ± 0.6	9
$Ca_v1.3_{42A}$	-29.0 ± 1.3^c	-6.5 ± 0.3^a	-14.0 ± 1.5^c	57.4 ± 1.5	-50.2 ± 0.7	12

[a] $p < 0.01$, comparison with $Ca_v1.3_L$. One-way ANOVA followed by Bonferroni post test.
[b] $p < 0.05$, comparison with $Ca_v1.3_L$. One-way ANOVA followed by Bonferroni post test.
[c] $p < 0.001$, comparison with $Ca_v1.3_L$. One-way ANOVA followed by Bonferroni post test.

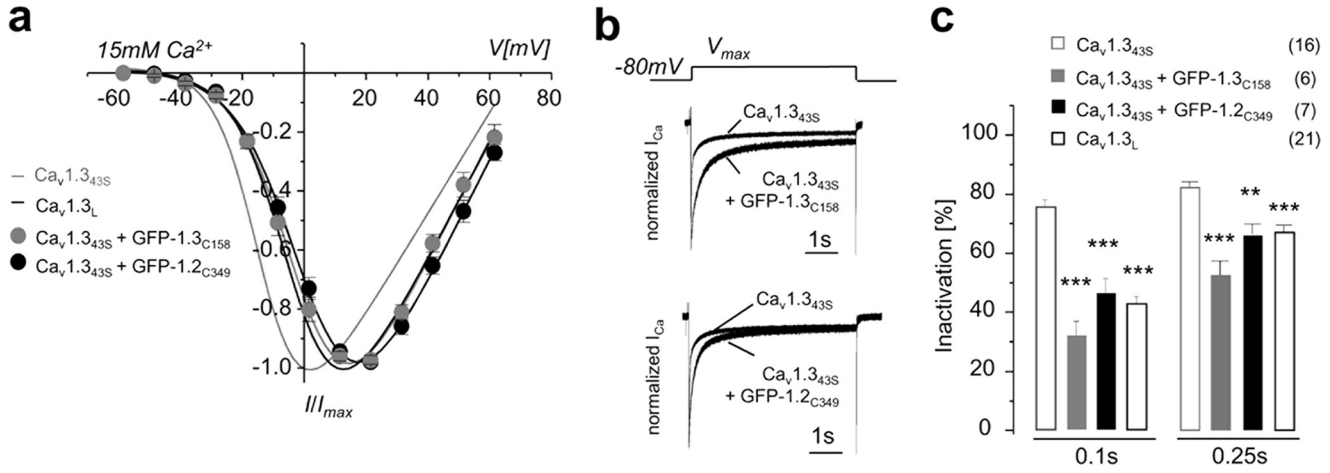

FIGURE 7. **Changes in $Ca_V1.3_{43S}$ channel gating properties in the presence of distal $Ca_V1.3$ or $Ca_V1.2$ C-terminal peptides.** *a*, mean normalized *I-V* curves recorded in tsA-201 cells expressing $Ca_V1.3_{43S}$ GFP-labeled peptides 1.3_{C158} (*gray dots*) and 1.2_{C349} (*black dots*); *I-V* curves for $Ca_V1.3_{43S}$ and $Ca_V1.3_L$ are depicted as *gray* and *black fitted lines*, respectively. Activation parameters of $Ca_V1.3_{43S}$ + C-terminal peptides were not statistically significant from $Ca_V1.3_L$. For statistically significant differences, see Table 1. *b*, normalized peak currents evoked by 5-s depolarizing steps to V_{max}. *c*, percent I_{Ca} inactivation was calculated during 0.1–0.25-s test pulses to V_{max}. Number of experiments is given in *parentheses*. *Error bars* reflect S.E. **, $p < 0.01$; ***, $p < 0.001$ compared with $Ca_v1.3_{43S}$, one-way ANOVA was followed by Bonferroni post test.

extracellular Ca^{2+} concentration. For differences in time constants see the legend to Fig. 8.

Taken together, our data demonstrate that C-terminal alternative splicing caused differences in the dynamics of Ca^{2+} influx during patterns of channel activity observed in neurons. In accordance with the observation that $Ca_v1.3_{43S}$ and $Ca_v1.3_{42A}$ are prominently expressed together with $Ca_v1.3_L$ in the SN this suggests that they may contribute differentially to Ca^{2+} signaling, depending on the activity state of the cell.

DISCUSSION

Our work provides important new insight into the tight control of the C-terminal modulatory domain of $Ca_v1.3$ channels. We discovered $Ca_v1.3_{43S}$ as a new, abundant $Ca_v1.3$ variant

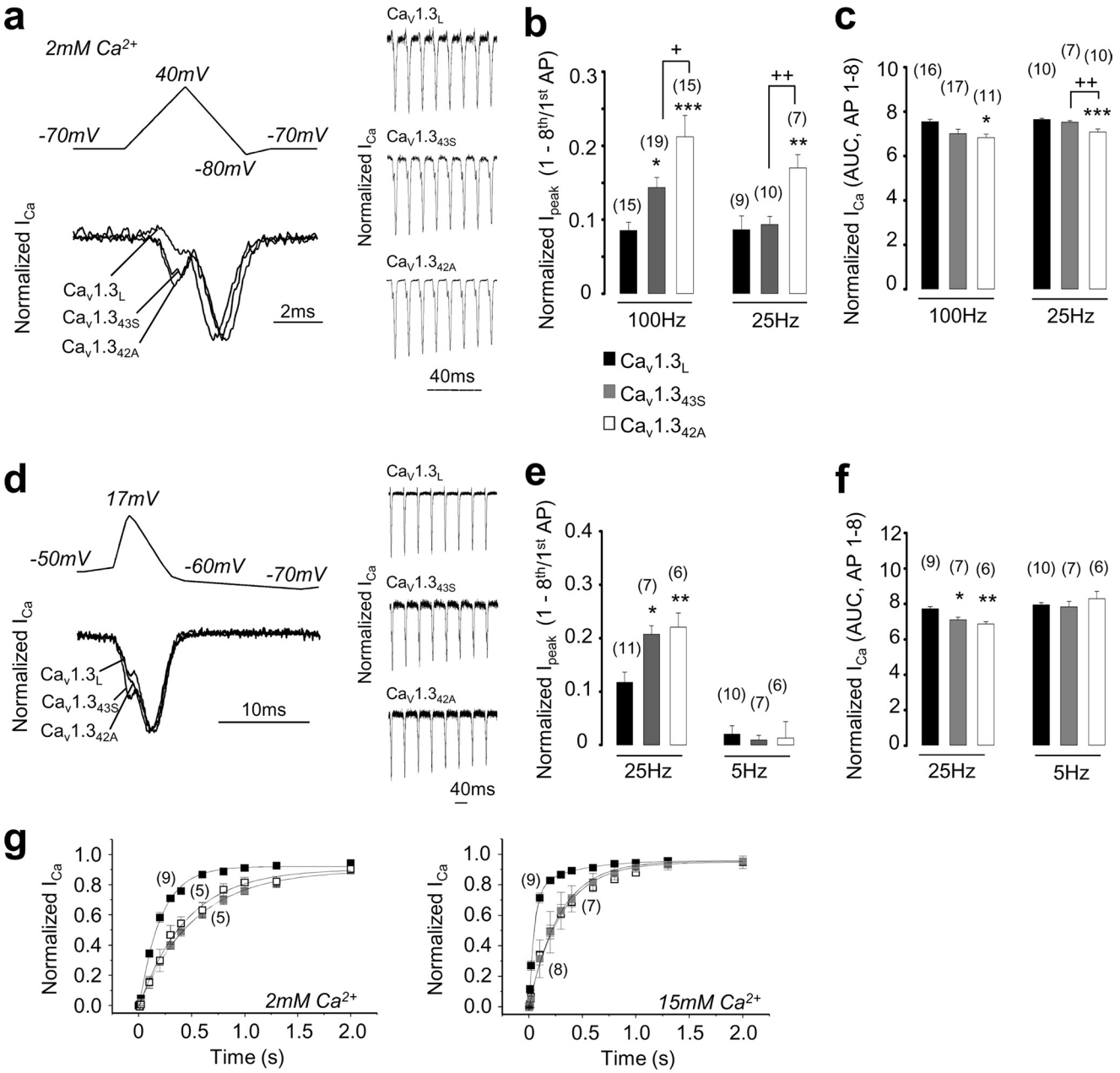

FIGURE 8. **Activity-dependent I_{Ca} through $Ca_v1.3$ α1 subunit splice variants during APW-like stimuli.** All experiments shown in *a-f* were recorded using 2 mM Ca^{2+} as charge carrier. *a*, *top*, APW voltage protocol elicited from −70 to +40, +40 to −80, and −80 to −70 mV (afterhyperpolarization). *Bottom*, normalized I_{Ca} in response to first APW for $Ca_v1.3_L$, $Ca_v1.3_{43S}$, and $Ca_v1.3_{42A}$ (cells: $Ca_v1.3_L$, 251010_95; $Ca_v1.3_{43S}$, 221110_133; $Ca_v1.3_{42A}$, 291010_78). *Right*: the I_{Ca} response to eight APWs elicited at 100-Hz is shown for representative experiments (cells: $Ca_v1.3_L$, 251010_128; $Ca_v1.3_{43S}$, 251010_5; $Ca_v1.3_{42A}$, 151110_187). *b*, decrease of the I_{peak} during 100- and 25-Hz trains expressed as the ratio of I_{peak} after the 8th stimulus divided by the I_{peak} of the first APW. *c*, normalized integrated I_{Ca} (AUC) throughout eight 100- and 25-Hz trains (I_{Ca} during first APW was normalized to 1). *, $p < 0.05$; **, $p < 0.01$; ***, $p < 0.001$ comparison to $Ca_v1.3_L$, + and ++ comparison between $Ca_v1.3_{43S}$ and $Ca_v1.3_{42A}$; *d*, *top,* voltage protocol of (SNc)-like APWs. *Bottom*, I_{Ca} in response to first APW for $Ca_v1.3_L$, $Ca_v1.3_{43S}$, and $Ca_v1.3_{42A}$ α1 subunits; *curves* reflect the mean from all experiments each normalized to I_{peak}. *Right,* I_{Ca} response to eight APWs elicited at 25 Hz is shown for representative experiments (cells: $Ca_v1.3_L$, 151210_43; $Ca_v1.3_{43S}$, 101210_250; $Ca_v1.3_{42A}$, 101210_140). *e* and *f* are as described in *b* and *c* for (SNc)-like APWs. *g*, recovery of I_{Ca} inactivation in 2 mM (*left*) and 15 mM Ca^{2+} (*right*) for $Ca_v1.3_L$, $Ca_v1.3_{43S}$, and $Ca_v1.3_{42A}$. Recovery curves were best fitted with a bi- ($Ca_v1.3_L$) or monoexponential function (short variants) yielding the following time constants (τ, in ms): 15 mM Ca^{2+}, $Ca_v1.3_L$, τ_{fast}, 47.4 ± 3.4; τ_{slow}, 385.5 ± 105; 78% τ_{fast}, $Ca_v1.3_{43S}$, τ = 300 ± 14.2; $Ca_v1.3_{42A}$, τ = 284 ± 7.5; 2 mM Ca^{2+}, $Ca_v1.3_L$, τ_{fast}, 150 ± 102.5, τ_{slow}, 336 ± 367.6, 57% τ_{fast}, $Ca_v1.3_{43S}$: τ = 448.3 ± 14.2, $Ca_v1.3_{42A}$, τ = 519.3 ± 8.2. Data are given as mean ± S.E. All statistical comparisons were made using one-way ANOVA and Bonferroni post test.

with preferential expression in the brain. Although $Ca_v1.3_{43S}$ channels are devoid of a functional CTM and show short gating behavior, the fact that these channels contain an additional sequence after the IQ CaM interaction motif including the PCRD domain induced gating behavior significantly different from $Ca_v1.3_{42A}$. We provide direct evidence in single channel recordings that the presence of the $Ca_v1.3$-CTM causes a strong reduction of the P_{open} of the channel. Moreover, we demonstrate that alternative splicing in the C terminus significantly changes the dynamics of $Ca_v1.3$-mediated Ca^{2+} entry during electrical activity mimicking different neuronal firing patterns.

Our discovery of $Ca_v1.3_{43S}$ now defines four classes of functionally distinct $Ca_v1.3$ channel variants generated by alternative splicing in the C terminus. One class of $Ca_v1.3$ channels lacks a functional IQ domain that is a major site for CaM interaction (30). This class results from a frameshift in exon 41 caused by different acceptor site usage and is expressed in the inner ear (31) as well as in pancreatic islets (32). CaM-mediated CDI is absent in this variant (31). Notably, we report here two new splice variants expressed in human and mouse brain that also lack a functional IQ domain but result from the omission of exon 41 and direct linking of exon 40 with either exon 42 or 42A. We did not further characterize these transcripts in this study. A second and third class corresponds to $Ca_v1.3_L$ and $Ca_v1.3_{42A}$ channels that either contain or completely lack the two CTM domains (PCRD and DCRD) (8). $Ca_v1.3_{43S}$ channels define a new fourth class, because they still contain the PCRD domain. Despite biophysical properties very similar to $Ca_v1.3_{42A}$ we found several differences between these two short forms: the P_{open} of $Ca_v1.3_{43S}$ differed from $Ca_v1.3_{42A}$ at physiologically relevant test potentials, CDI in $Ca_v1.3_{43S}$ channels was less pronounced with 2 mM Ca^{2+} as the charge carrier, and compared with $Ca_v1.3_L$ 25 Hz APWs from −70 mV caused a more pronounced peak current decay during brief trains in $Ca_v1.3_{42A}$ but not in $Ca_v1.3_{43S}$ channels. These data indicate that either the presence of the PCRD or the additional 15-amino acid peptide forming a unique C terminus (Fig. 1*a*) can still exert functional effects on channel gating. The molecular mechanism, however, still needs to be clarified. Interference of this sequence stretch with CaM binding/effector sites that are located adjacent to the PCRD domain is one possible explanation for the slight moderation of CDI in $Ca_v1.3_{43S}$ channels.

Another distinguishing feature of $Ca_v1.3_{43S}$ is its capability to bind peptides containing the DCRD and thereby form a fully functional CTM. We show that this is not limited to the DCRD of $Ca_v1.3$ channels because a peptide with a $Ca_v1.2$-derived DCRD also induced gating properties indistinguishable from the long form of $Ca_v1.3$. Although C-terminal proteolytical processing has not been detected so far for $Ca_v1.3$ channels, the C termini of both $Ca_v1.1$ (skeletal muscle (33)) and $Ca_v1.2$ (brain (25, 34) and heart (24, 35)) are post-translationally cleaved. The $Ca_v1.2$ fragment either remains noncovalently associated with the channel (24) or exists as a separate peptide that can translocate to the nucleus from the cytoplasm in an activity-dependent manner (25). It is therefore possible that this peptide also binds to $Ca_v1.3_{43S}$ either via a potential signaling link between $Ca_v1.2$ and $Ca_v1.3$ channels or even via a nuclear signaling pathway. Our findings therefore provide a rational basis for further biochemical experiments to prove the existence of such complexes *in vivo*. However, one has to take into account that this would require immunoprecipitation experiments with specific antibodies directed against $Ca_v1.3_{43S}$ employing extracts from a (limited) subset of brain regions where the cleaved fragment is most abundant (25).

Our quantitative and semi-quantitative PCR data revealed that the two short variants are primarily expressed in mouse and human brain but occur at much lower abundance in heart. Previous work was based on the assumption that inclusion of exon 42A results in $Ca_v1.3$ variants with short C termini, whereas inclusion of exon 42 invariably results in a long C terminus encoded by exons 42 to 49 (with or without exon 44, (8)). Here we demonstrate that exon 42 may also be part of the short variant $Ca_v1.3_{43S}$. If exon 42 can be linked to either 43 (permitting long transcripts) or 43S, and if there is no further truncating splicing downstream, then the sum of full-length transcripts (reflected by the abundance of exon 49) and transcripts containing 43S should approximately equal the number of transcripts containing exon 42. In whole brain this appears to be the case, because we found that at least 39% of exon 43-derived transcripts comprise 43S, and exon 49 is abundantly expressed (Fig. 1, *a* and *b*). A larger discrepancy was found in the SAN. Less than 10% of transcripts in SAN contained 43S, suggesting that in the heart exon 42 preferentially combines with long exon 43. Thus, there should be predominant abundance of full-length transcripts. However, exon 49 as our full-length transcript "indicator" was also not very abundant in the SAN, and exons 42A + 49 did not add up to the exon 42 expression level (Fig. 1*b*). This indicates that one or more yet unidentified splice variants (presumably with short gating characteristics) might exist in the SAN. In a numerical modeling of mouse SAN automaticity (supplemental Fig. S2) we showed that I_{Ca} mediated by both $Ca_v1.3_L$ and $Ca_v1.3_{42A}$ can sustain pacemaking when using the biophysical properties of the two variants recorded in 2 mM extracellular Ca^{2+}. $Ca_v1.3_{42A}$-mediated I_{Ca} generated a SAN pacing rate that was slightly faster than that of $Ca_v1.3_L$ (supplemental Fig. S2). Simulation of I_{CaL} behavior during pacemaking showed the predicted current peak of $Ca_v1.3_L$-mediated I_{CaL} during the action potential plateau and the first repolarization phases were higher than that of $Ca_v1.3_{42A}$-mediated I_{CaL} (supplemental Fig. S2*b*). This prediction is consistent with the faster inactivation kinetics of $Ca_v1.3_{42A}$-mediated I_{CaL} and accounted for the slightly shorter action potential duration of $Ca_v1.3_L$-mediated pacemaking (supplemental Fig. S2*a*).

We also found pronounced differences for I_{Ca} mediated by the different splice variants during neuron-like activity patterns, in particular between long $Ca_v1.3_L$ and short forms. These differences were frequency dependent and mainly seen at higher stimulation rates. We predict that somatodendritic expression of short variants, associated with a more pronounced current decay during high frequency bursts (as suggested by our data), would cause smaller Ca^{2+} accumulation and may affect the strength and/or dynamics of other Ca^{2+}-dependent processes, in particular coupling to Ca^{2+}-activated K^+ channels (33, 36), excitation transcription coupling (2, 3), or Ca^{2+} release from intracellular stores (37). Such mechanisms may help a neuron to prevent an excessive increase in intracellular Ca^{2+} during bursting and be especially important, *e.g.* for SNc neurons in which $Ca_v1.3$ LTCCs have been found to contribute to their selective vulnerability in Parkinson disease (21) and where Ca^{2+} buffering capacity is low (38). These neurons have even been reported to switch from a low frequency rhythmic firing mode (up to around 5 Hz) to a bursting mode with 2–10 APs of higher frequency (up to 30 Hz) in response to unexpected presentation of primary rewards (29, 39). During burst activity intracellular Ca^{2+} is known to rise to much higher levels (37). We showed in this study that both short forms (in particular $Ca_v1.3_{42A}$) are expressed in the SNc in addition to the

long form. It will therefore be particularly interesting to examine the possibility of whether the ratio of these variants is also altered under pathophysiological conditions in the neurodegenerative process of Parkinson disease.

Acknowledgments—We thank Jenny Müller, Michaela Hatzl, and Gospava Stojanovic for excellent technical assistance.

Note Added in Proof—Splice variant Cav1.343S and additional C-terminal splice variants are described in an accompanying paper (40).

REFERENCES

1. Striessnig, J., and Koschak, A. (2008) *Channels* **2,** 233–251
2. Deisseroth, K., Mermelstein, P. G., Xia, H., and Tsien, R. W. (2003) *Curr. Opin. Neurobiol.* **13,** 354–365
3. Barbado, M., Fablet, K., Ronjat, M., and De Waard, M. (2009) *Biochim. Biophys. Acta* **1793,** 1096–1104
4. Jing, X., Li, D. Q., Olofsson, C. S., Salehi, A., Surve, V. V., Caballero, J., Ivarsson, R., Lundquist, I., Pereverzev, A., Schneider, T., Rorsman, P., and Renström, E. (2005) *J. Clin. Invest.* **115,** 146–154
5. Andrade, A., Denome, S., Jiang, Y. Q., Marangoudakis, S., and Lipscombe, D. (2010) *Nat. Neurosci.* **13,** 1249–1256
6. Liao, P., Yu, D., Li, G., Yong, T. F., Soon, J. L., Chua, Y. L., and Soong, T. W. (2007) *J. Biol. Chem.* **282,** 35133–35142
7. Singh, A., Hamedinger, D., Hoda, J. C., Gebhart, M., Koschak, A., Romanin, C., and Striessnig, J. (2006) *Nat. Neurosci.* **9,** 1108–1116
8. Singh, A., Gebhart, M., Fritsch, R., Sinnegger-Brauns, M. J., Poggiani, C., Hoda, J. C., Engel, J., Romanin, C., Striessnig, J., and Koschak, A. (2008) *J. Biol. Chem.* **283,** 20733–20744
9. Striessnig, J., Bolz, H. J., and Koschak, A. (2010) *Pflugers Arch.* **460,** 361–374
10. Olson, P. A., Tkatch, T., Hernandez-Lopez, S., Ulrich, S., Ilijic, E., Mugnaini, E., Zhang, H., Bezprozvanny, I., and Surmeier, D. J. (2005) *J. Neurosci.* **25,** 1050–1062
11. Platzer, J., Engel, J., Schrott-Fischer, A., Stephan, K., Bova, S., Chen, H., Zheng, H., and Striessnig, J. (2000) *Cell* **102,** 89–97
12. Sinnegger-Brauns, M. J., Huber, I. G., Koschak, A., Wild, C., Obermair, G. J., Einzinger, U., Hoda, J. C., Sartori, S. B., and Striessnig, J. (2009) *Mol. Pharmacol.* **75,** 407–414
13. Baig, S. M., Koschak, A., Lieb, A., Gebhart, M., Dafinger, C., Nürnberg, G., Ali, A., Ahmad, I., Sinnegger-Brauns, M. J., Brandt, N., Engel, J., Mangoni, M. E., Farooq, M., Khan, H. U., Nürnberg, P., Striessnig, J., and Bolz, H. J. (2011) *Nat. Neurosci.* **14,** 77–84
14. Tang, Z. Z., Liang, M. C., Lu, S., Yu, D., Yu, C. Y., Yue, D. T., and Soong, T. W. (2004) *J. Biol. Chem.* **279,** 44335–44343
15. Marcantoni, A., Vandael, D. H., Mahapatra, S., Carabelli, V., Sinnegger-Brauns, M. J., Striessnig, J., and Carbone, E. (2010) *J. Neurosci.* **30,** 491–504
16. Soong, T. W., DeMaria, C. D., Alvania, R. S., Zweifel, L. S., Liang, M. C., Mittman, S., Agnew, W. S., and Yue, D. T. (2002) *J. Neurosci.* **22,** 10142–10152
17. Grabner, M., Dirksen, R. T., and Beam, K. G. (1998) *Proc. Natl. Acad. Sci. U.S.A.* **95,** 1903–1908
18. Koschak, A., Reimer, D., Huber, I., Grabner, M., Glossmann, H., Engel, J., and Striessnig, J. (2001) *J. Biol. Chem.* **276,** 22100–22106
19. Jangsangthong, W., Kuzmenkina, E., Khan, I. F., Matthes, J., Hullin, R., and Herzig, S. (2010) *Pflugers Arch.* **459,** 399–411
20. Schröder, F., Handrock, R., Beuckelmann, D. J., Hirt, S., Hullin, R., Priebe, L., Schwinger, R. H., Weil, J., and Herzig, S. (1998) *Circulation* **98,** 969–976
21. Surmeier, D. J., Guzman, J. N., Sanchez-Padilla, J., and Goldberg, J. A. (2011) *Antioxid. Redox Signal.* **14,** 1289–1301
22. Chan, C. S., Guzman, J. N., Ilijic, E., Mercer, J. N., Rick, C., Tkatch, T., Meredith, G. E., and Surmeier, D. J. (2007) *Nature* **447,** 1081–1086
23. Xu, W., and Lipscombe, D. (2001) *J. Neurosci.* **21,** 5944–5951
24. Hulme, J. T., Yarov-Yarovoy, V., Lin, T. W., Scheuer, T., and Catterall, W. A. (2006) *J. Physiol.* **576,** 87–102
25. Gomez-Ospina, N., Tsuruta, F., Barreto-Chang, O., Hu, L., and Dolmetsch, R. (2006) *Cell* **127,** 591–606
26. Lisman, J. E. (1997) *Trends Neurosci.* **20,** 38–43
27. Moosmang, S., Haider, N., Klugbauer, N., Adelsberger, H., Langwieser, N., Müller, J., Stiess, M., Marais, E., Schulla, V., Lacinova, L., Goebbels, S., Nave, K. A., Storm, D. R., Hofmann, F., and Kleppisch, T. (2005) *J. Neurosci.* **25,** 9883–9892
28. Helton, T. D., Xu, W., and Lipscombe, D. (2005) *J. Neurosci.* **25,** 10247–10251
29. Liss, B., and Roeper, J. (2008) *Brain Res. Rev.* **58,** 314–321
30. Erickson, M. G., Liang, H., Mori, M. X., and Yue, D. T. (2003) *Neuron* **39,** 97–107
31. Shen, Y., Yu, D., Hiel, H., Liao, P., Yue, D. T., Fuchs, P. A., and Soong, T. W. (2006) *J. Neurosci.* **26,** 10690–10699
32. Ihara, Y., Yamada, Y., Fujii, Y., Gonoi, T., Yano, H., Yasuda, K., Inagaki, N., Seino, Y., and Seino, S. (1995) *Mol. Endocrinol.* **9,** 121–130
33. Hulme, J. T., Konoki, K., Lin, T. W., Gritsenko, M. A., Camp, D. G., 2nd, Bigelow, D. J., and Catterall, W. A. (2005) *Proc. Natl. Acad. Sci. U.S.A.* **102,** 5274–5279
34. Hell, J. W., Westenbroek, R. E., Breeze, L. J., Wang, K. K., Chavkin, C., and Catterall, W. A. (1996) *Proc. Natl. Acad. Sci. U.S.A.* **93,** 3362–3367
35. De Jongh, K. S., Murphy, B. J., Colvin, A. A., Hell, J. W., Takahashi, M., and Catterall, W. A. (1996) *Biochemistry* **35,** 10392–10402
36. Berkefeld, H., and Fakler, B. (2008) *J. Neurosci.* **28,** 8238–8245
37. Cui, G., Bernier, B. E., Harnett, M. T., and Morikawa, H. (2007) *J. Neurosci.* **27,** 4776–4785
38. Foehring, R. C., Zhang, X. F., Lee, J. C., and Callaway, J. C. (2009) *J. Neurophysiol.* **102,** 2326–2333
39. Blythe, S. N., Wokosin, D., Atherton, J. F., and Bevan, M. D. (2009) *J. Neurosci.* **29,** 15531–15541
40. Tan, B. Z., Jiang, F., Tan, M. Y., Yu, D., Huang, H., Shen, Y., and Soong, T. W. (2011) *J. Biol. Chem.* **286,** 42725–42735